Current Research in Structural Biology 2 (2020) 180–190

Contents lists available at ScienceDirect

Current Research in Structural Biology

journal homepage: www.journals.elsevier.com/current-research-in-structural-biology

Structure dictates the mechanism of ligand recognition in the histidine and maltose binding proteins

Lakshmi P. Jayanthi [a,1], Nahren Manuel Mascarenhas [b,**,1], Shachi Gosavi [a,*]

[a] Simons Centre for the Study of Living Machines, National Centre for Biological Sciences, Tata Institute of Fundamental Research, Bangalore, 560065, India
[b] Department of Chemistry, Sacred Heart College (Autonomous), Tirupattur, 635601, India

ARTICLE INFO

Keywords:
Conformational selection
Induced fit
Periplasmic binding proteins
Structural restraints
Dual structure based models
MD simulations

ABSTRACT

Two mechanisms, induced fit (IF) and conformational selection (CS), have been proposed to explain ligand recognition coupled conformational changes. The histidine binding protein (HisJ) adopts the CS mechanism, in which a pre-equilibrium is established between the open and the closed states with the ligand binding to the closed state. Despite being structurally similar to HisJ, the maltose binding protein (MBP) adopts the IF mechanism, in which the ligand binds the open state and induces a transition to the closed state. To understand the molecular determinants of this difference, we performed molecular dynamics (MD) simulations of coarse-grained dual structure based models. We find that intra-protein contacts unique to the closed state are sufficient to promote the conformational transition in HisJ, indicating a CS-like mechanism. In contrast, additional ligand-mimicking contacts are required to "induce" the conformational transition in MBP suggesting an IF-like mechanism. In agreement with experiments, destabilizing modifications to two structural features, the spine helix (SH) and the balancing interface (BI), present in MBP but absent in HisJ, reduce the need for ligand-mimicking contacts indicating that SH and BI act as structural restraints that keep MBP in the open state. We introduce an SH like element into HisJ and observe that this can impede the conformational transition increasing the importance of ligand-mimicking contacts. Similarly, simultaneous mutations to BI and SH in MBP reduce the barrier to conformational transitions significantly and promote a CS-like mechanism. Together, our results show that structural restraints present in the protein structure can determine the mechanism of conformational transitions and even simple models that correctly capture such structural features can predict their positions. MD simulations of such models can thus be used, in conjunction with mutational experiments, to regulate protein ligand interactions, and modulate ligand binding affinities.

1. Introduction

Proteins function by binding other molecules and this binding is often associated with protein dynamics (Henzler-Wildman and Kern, 2007; Grant et al., 2010; Amemiya et al., 2012). Characterizing the nature of such ligand associated conformational dynamics in terms of structure, kinetics and energetics is essential for understanding key cellular processes. This knowledge is also necessary for biotechnological applications such as rational structure based drug and sensor design (Medintz and Deschamps, 2006; Ribeiro et al., 2019; Lukman et al., 2014). Two distinct mechanisms, namely, conformational selection (CS) and induced fit (IF) have been proposed to describe ligand-binding associated conformational changes (Monod et al., 1965; Koshland et al., 1966; Hammes et al., 2009). In CS, the protein exists in an equilibrium between the 'open' (or unbound or apo) and the 'closed' (or bound or holo) conformational states. The ligand binds to the closed conformation and shifts the conformational equilibrium to this state (Fig. 1A). Thus, the conformational change is intrinsic to the protein and not induced by the ligand. In contrast, in IF, the ligand interacts with the open state and the ligand protein interactions induce the protein to access the closed state

Abbreviations: BI, Balancing interface; CS, conformational selection; sSBM, single structure-based model; dSBM, dual structure-based model; HisJ, histidine binding protein; IF, induced fit; MBP, maltose binding protein; MD, molecular dynamics; SH, spine helix; WT, wild-type; NTD, N-terminal domain; CTD, C-terminal domain; PBP, periplasmic binding protein; FEP, free energy profile.

* Corresponding author.
** Corresponding author.
E-mail addresses: mailnahren@gmail.com (N.M. Mascarenhas), shachi@ncbs.res.in (S. Gosavi).
[1] These authors contributed equally.

https://doi.org/10.1016/j.crstbi.2020.08.001
Received 15 May 2020; Received in revised form 26 July 2020; Accepted 6 August 2020

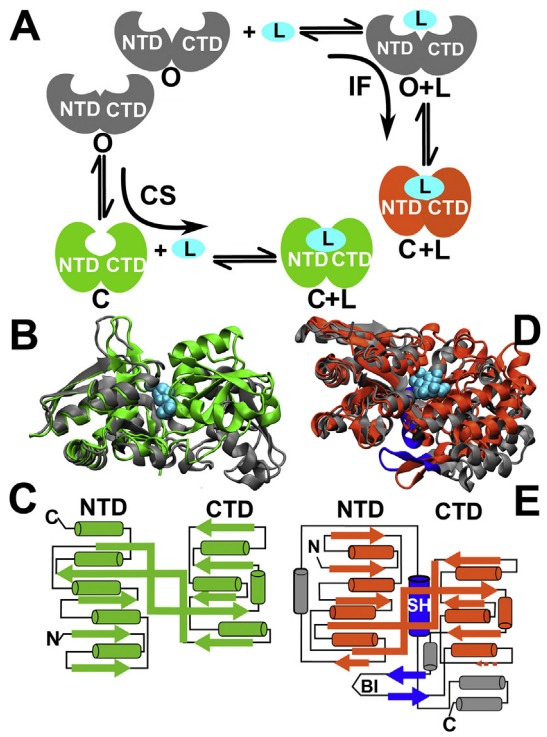

Fig. 1. Conformational transitions and structures of HisJ and MBP. (A) The ligand (cyan ellipse) binds to the protein (orange and green cartoons with the C-Terminal and N-Terminal Domains marked) before the conformational transition (O→C) in IF, while it binds to the protein after the conformational transition in CS. O is the open state, C is the closed state. (B) The aligned structures of the open (PDB ID: 2M8C; grey) and the ligand bound closed states of HisJ (PDB ID: 1HSL, chain B; green). The ligand is drawn with cyan spheres. (C) The splay diagram of HisJ. Helices are shown as cylinders and β-strands are drawn as arrows. The N- and C-termini are marked. (D) The aligned structures of the open (PDB ID: 1OMP; grey and blue) and the ligand bound closed states of MBP (PDB ID: 1ANF; orange). The ligand is drawn with cyan spheres. BI and SH, structural elements that restrain the movement from the open to the closed states, are marked in blue in the open structure and lie behind the ligand binding pocket. The position of the domains in the open states bring BI (the loop at the bottom of the cartoon) closer to the NTD. (E) The splay diagram of MBP. Helices are shown as cylinders and β-strands are drawn as arrows. The N- and C-termini are marked. As in D, BI and SH are shown in blue. Other structural elements present in MBP but absent in HisJ are marked in grey.

(Fig. 1A). A mixture of the two mechanisms has also been shown in some proteins, where an equilibrium between the open and a semi-closed state exists with the ligand binding to the semi-closed state inducing it to convert to the closed state (Silva et al., 2011).

Protein simulations have shown that ligands with stronger and longer-ranged ligand-protein interactions may be able to induce conformational changes in proteins more easily (Okazaki and Takada, 2008). Kinetic analyses of both experimental and simulation data have also led to insights into ligand coupled conformational dynamics (Weikl and Von Deuster, 2009; Paul and Weikl, 2016; Chakraborty and Di Cera, 2017). Specifically, it has been shown that lower ligand concentrations as well as lower rates of protein dynamics lead to a CS like mechanism while higher concentrations of ligand and rates of protein dynamics can lead to an IF like mechanism (Greives and Zhou, 2014; Zhou, 2010; Cai and Zhou, 2011). However, in the cellular milieu ligand concentrations are likely to be regulated and features intrinsic to the protein structure may determine the mechanism of conformational transitions. Here, we investigate this hypothesis using two structurally similar periplasmic binding proteins (PBPs), histidine binding protein (HisJ) and maltose binding protein (MBP), whose conformational transitions occur by the two different mechanisms.

PBPs are located in the periplasmic regions of gram negative bacteria, bind to a wide variety of ligands and are involved in the transport of these solutes across the cytoplasmic membrane (Quiocho and Ledvina, 1996; Ames, 1986; Scheepers et al., 2016; Felder et al., 1999). They usually have two domains (or lobes), often termed the N-terminal domain (NTD) and the C-terminal domain (CTD), interlinked by one or more flexible peptide linkers. The ligand binding site is located at the cleft between the two domains. Linker (or hinge) flexibility facilitates domain motion, allowing the proteins to switch between different conformations. The conformational adaptability of PBPs has been used in the development of biosensors and biologically active receptors (Medintz and Deschamps, 2006; Allert et al., 2004; Nadler et al., 2016). Therefore, understanding the structural basis of ligand-coupled conformational transitions in the PBPs will enable the development of sensors with bespoke binding specificities.

One of the smaller PBPs, the 241 amino acid HisJ, is a part of the periplasmic histidine transport chain. It has a canonical PBP structure with two linkers, connecting its two domains (Fig. 1B and C). A sensor based on HisJ has already been used to track histidine concentrations in cells (Hu et al., 2017). HisJ also binds other positively charged amino acids with differing binding affinities (Paul et al., 2017) making it a target for binding site redesign. Experimental studies indicate that HisJ interconverts between its open and closed states even in the absence of the ligand (Wolf et al., 1994). Recent molecular dynamics simulations have also demonstrated that unbound HisJ can transition to the closed state (Chu et al., 2014). This implies that the conformational transition in HisJ precedes ligand binding suggesting a CS-like mechanism.

The 370 amino acid MBP (Fig. 1D and E) can bind several sugars with differing binding affinities (Miller et al., 1983; Ferenci, 1980; Sharff et al., 1993). The two domains of MBP are connected by three linkers: two β-strands and a short helix called the spine helix, which lies behind the binding cleft (Fig. 1E). MBP has been widely used as a solubility and affinity tag (Kapust and Waugh, 1999; di Guana et al., 1988). Its properties have also been tuned to create several biosensors (Medintz and Deschamps, 2006; Marvin and Hellinga, 2001a). Molecular simulations have been used to investigate several important questions about the conformational transitions of MBP including which residues contribute to ligand recognition, water mediated interactions and domain closure and whether MBP transitions to the closed state in the absence of ligand (Stockner et al., 2005; Huang et al., 2015; Bucher et al., 2011a,b). Although a minor semi-closed state (population ~5%) was detected for MBP using nuclear magnetic resonance (NMR) spectroscopy (Tang et al., 2007), analyses of both simulations (Stockner et al., 2005; Kondo et al., 2011) and single molecule Förster resonance energy transfer (smFRET) traces (Kim et al., 2013; De Boer et al., 2019) concluded that this off-pathway intermediate did not affect the ligand coupled conformational transitions which proceeded predominantly through the IF mechanism. Henceforth, we do not include this semi-closed state in our models and analyses.

Although MBP and HisJ have a similar overall topology (Fig. 1B–E), structural differences exist which could influence the mechanism of conformational transitions. Mechanical unfolding studies have shown that such structural differences can even result in changes in global dynamics with different unfolding behavior, i.e., two and three state unfolding, being observed across the PBP family (Kotamarthi et al., 2014; Aggarwal et al., 2011). A comparison of the topologies of HisJ (Fig. 1C) and MBP (Fig. 1E) highlights the presence of two structural modules that lie behind the binding pocket in MBP but which are absent in HisJ, namely the spine helix (SH; residues K313-M330) and the balancing interface (BI; residues K170-D180). Several experimental and simulation studies have showed that these two modules anchor MBP in the open state (Bucher et al., 2011a,b; Telmer and Shilton, 2003; Walker et al., 2010; Marvin and Hellinga, 2001; Millet et al., 2003; Mascarenhas and Kästner, 2013; Wang et al., 2012; Seo et al., 2014). Contact calculations, detailed in the methods section, also indicate that the residues of BI and

SH are involved in several interactions in the open state which break in the closed-state (Supplementary Information).

Here, we examine whether the absence of these structural anchors promotes the CS mechanism in HisJ and whether their presence enables the IF mechanism in MBP, by using coarse-grained dual structure-based models (dSBMs) and molecular dynamics (MD) simulations. dSBMs encode structural information from both the open and the closed states. MD simulations of such models enable extensive sampling of the conformational transition and have been successfully used to describe both the folding and the functional transitions of proteins (Baxter et al., 2012; Whitford et al., 2007; Giri Rao et al., 2016; Okazaki et al., 2006; Ramírez-Sarmiento et al., 2015; Best et al., 2005). We find that dSBMs correctly capture the mechanism of conformational transitions in both HisJ and MBP. Specifically, intra-protein closed state interactions are sufficient to enable the conformational conversion of HisJ. In contrast, BI and SH act as structural restraints in MBP and in addition to closed state interactions, ligand mediated contacts are also needed to induce the conformational transitions of MBP. Finally, we show that the ligand coupled conformational dynamics of both HisJ and MBP can be modulated through the addition or deletion of appropriate structural restraints.

2. Results

2.1. Dual structure-based models of HisJ and MBP

Conformational transitions occur on timescales still not routinely accessible to all-atom molecular dynamics (MD) simulations with the required computational power escalating with the size of the protein. One solution to this problem is to use coarse-grained structure-based models which simplify the potential energy function and enable extensive sampling of the free energy landscape of the protein. Dual structure-based models (dSBMs) assume that the mechanism of conformational transitions depends solely on the two end structures (e.g. the open and the closed states) and have been successful at capturing the conformational free energy landscapes of proteins (Whitford et al., 2007; Giri Rao et al., 2016; Okazaki et al., 2006; Ramírez-Sarmiento et al., 2015). To simulate the conformational transition, dSBMs encode structural data from the two endpoints of the transition in their potential energy functions. Generally, one of the structures, usually the open structure is encoded completely. However, the amount of information encoded from the second structure depends on the nature of the conformational transition with different flavors of dSBMs including everything from only a few contacts from the second structure (Whitford et al., 2007) to including both structures equally (Giri Rao et al., 2016). The construction of dSBMs is further discussed in the first subsection of Discussion.

In proteins like adenylate kinase (Whitford et al., 2007), MBP (Wang et al., 2012) and glutamine binding protein (Okazaki et al., 2006), in which conformational transitions involve the relative motion of entire domains about a small number of hinge residues with little change in secondary structure, it is sufficient to include only a few contacts calculated from the closed state in the dSBM. To verify that such a dSBM would also be sufficient for both HisJ and MBP, we compared the dihedral angles formed by the Cα atoms of four successive residues in the open and the closed states of both proteins. We found, for both proteins, that the dihedral angles do not vary appreciably between the two states except in the hinge regions indicating that the secondary structure remains mostly unchanged. Thus, we use a dSBM which includes only a few contacts from the closed state structure to understand the mechanistic differences between the ligand associated conformational changes in HisJ and MBP. It should be noted that secondary structural elements (e.g. α-helices) in the hinge regions can locally unfold or "crack" in dSBM simulations even when dihedrals are calculated from a single structure (Whitford et al., 2007). The loss of stability due to such local unfolding is usually compensated for by the formation of the closed-state specific contacts.

To construct the dSBM, we first define a single structure-based model (sSBM) using the open conformations of each protein (Fig. 1B and D) and then add to this sSBM a perturbation in the form of scaled closed state or ligand mediated contacts which drive the conformational change. Consequently, three types of contacts are present in the simulations: (1) Open state contacts: Many of these are also incidentally present in the closed state, (2) Closed state contacts: These are specific to the closed state and absent in the open state and (3) Ligand mediated contacts: These ligand-mimicking contacts are present between pairs of residues both of which are in contact with the ligand in the closed state. So, the ligand is included implicitly through these contacts. In order to use a minimal set of contacts, we use only inter-domain contacts for both closed state and ligand mediated contacts. Details of the contact calculations and the dSBM are given in the Methods section. MD simulations of the dSBMs were then used to gain insights into the structural modules that determine the mechanisms of conformational transitions. We first ask if dSBMs can capture the mechanism of conformational transitions for HisJ (CS) and MBP (IF).

2.2. Intra-protein contacts promote transition to the closed state in HisJ but not in MBP

The closed state is populated in the absence of the ligand in the CS mechanism. In order to test for CS, we removed the ligand from the closed states of the proteins and calculated intra-protein contacts which are specific to the closed states (Q_C). As an example, some Q_C contacts are present along the binding pocket (Fig. 2A). If addition of only the Q_C contacts at scaled strengths (ε_C) can enable the conformational transition, then interactions present only within the protein are required for the conformational transition and an equilibrium between the open and closed states can be achieved even when the ligand is absent. We first performed dSBM MD simulations with Q_C to test whether these contacts are sufficient to enable a conformational change in HisJ and in MBP.

The distance between residues D53 and G119 was chosen as a proxy for the inter-domain distance in HisJ and served as the reaction coordinate to monitor the conformational transition (see Methods). The free energy profile (FEP) is the negative logarithm of the number of states populated at a specific inter-domain distance plotted as a function of the distance. A minimum in an FEP indicates a large population while a hump implies a transition state. Fig. 3A shows the FEP for HisJ with the strength of Q_C, ε_C, scaled to 1.5 times the strength of the open state contacts. Two minima at distances similar to those in the open and the closed states are observed, separated by a single barrier. This implies that closed state contacts are sufficient to promote conformational transitions in HisJ in dSBM simulations and the mechanism of conformational transitions in HisJ is indeed CS-like.

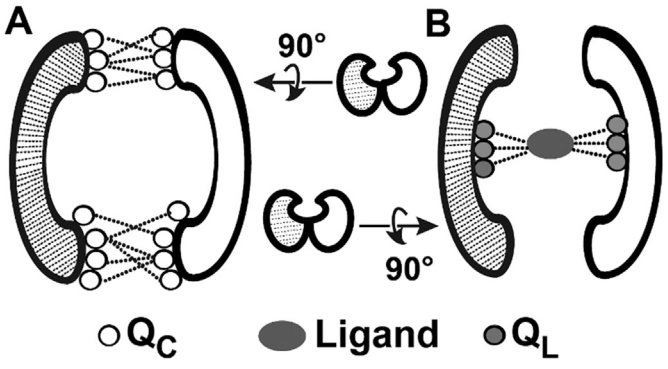

Fig. 2. Top views of the binding pocket and two sets of contacts. (A) Q_C (broken lines linking open circles) are contacts formed only in the Closed state. (B) Q_L (lines linking filled circles) are Ligand mediated contacts formed between the two domains of the proteins in the closed state. The effect of the ligand was included implicitly into the model through Q_L. The grey oval represents the ligand. The NTD is hatched, the CTD is unfilled.

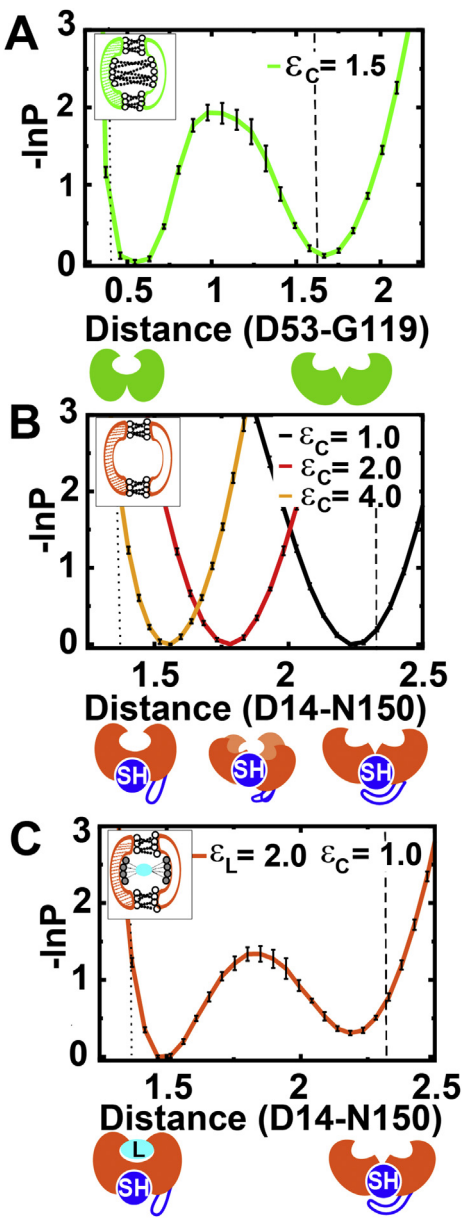

(caption on next column)

Fig. 3. Conformational transitions of HisJ and MBP. The free energy (-lnP) is plotted as a function of distance between inter-domain residues D53 and G119 in HisJ and D14 and N150 in MBP. The vertical dashed (open state; HisJ: 1.66 nm; MBP: 2.30 nm) and dotted (closed state; HisJ: 0.39 nm; MBP: 1.36 nm) lines mark the distance between these residues in the respective crystal structures. The error bars shown in black represent the standard deviation of the free energy profile (FEP). Cartoons of populated structures (HisJ in green and MBP in orange) are shown below the basins. The approximate location and types of contacts within the binding pocket present in each of the simulations is shown in the inset cartoon. (A) HisJ: The closed state contacts (Q_C) at a strength, $\varepsilon_C = 1.5$, are sufficient to promote conformational transitions and both the open (minimum at ~1.68 nm) and the closed (~0.55 nm) basins are populated. Several closed state contacts are present in HisJ and they line the binding pocket. (B) MBP: The closed state contacts are not sufficient to induce the conformational transition in MBP. A single partially closed ensemble at a distance intermediate between the open and the closed states is populated and an increase in the strength of Q_C (black: $\varepsilon_C = 1$, minimum at ~2.25 nm; red: $\varepsilon_C = 2$, minimum at ~1.80 nm; orange:$\varepsilon_C = 4$, minimum at ~1.57 nm) only induces increased closing. Few closed state contacts are present in MBP and these are located at the edges of the binding pocket. The structural restraints, BI (blue loop) and SH, that prevent the complete transition are shown in the cartoons below. (C) MBP: Addition of the ligand mediated contacts, Q_L, at a strength of $\varepsilon_L = 2.0$ to the Q_C at a strength of $\varepsilon_C = 1.0$ can induce the conformational transition in MBP and both the open (minimum at ~2.21 nm) and the closed state (~1.50 nm) basins are populated. The additional Q_L are located at the center of the binding pocket, with the ligand shown in cyan. Several interactions of both SH and BI (blue loop: extended towards the NTD in the open state) are broken in the closed state and this is depicted in the cartoons below. Although the ligand is shown in both the inset and the cartoon below, it is included only implicitly into the model through Q_L, contacts between those pairs of residues which are bridged by the ligand in the closed state.

The distance between residues D14 and N150 was chosen as a proxy for the inter-domain distance in MBP. Three FEPs of MBP are shown in Fig. 3B with varying strength of Q_C. Although, the position of the minimum decreases to smaller distances with increasing Q_C strengths only a single minimum is seen in each of the FEPs. Thus, with increasing strengths of closed state contacts, MBP shows increasing partial closure reminiscent of down-hill folding (Muñoz, 2007). However, complete closure is not seen even with contact strengths unrealistically larger than those of the open state contacts. Thus, closed state contacts are not sufficient to enable MBP to access its closed state.

2.3. Ligand mimicking contacts are necessary to induce a transition in MBP

In the closed ligand bound conformation of MBP, the ligand atoms interact with residues that line the binding pocket. Many of these ligand contacting residues are not directly in contact with each other through Q_C. However, the ligand provides an interaction bridge between some of these residues and we term such bridging contacts, ligand mediated contacts (Q_L; Fig. 2B; see Methods for contact calculations). We test if the addition of Q_L with the scaled strength, ε_L, and the previously calculated Q_C with the scaled strength, ε_C, can together induce a conformational transition in MBP. We set $\varepsilon_C = 1.0$, so that all intra protein contacts (both open and closed state) have the same strength, and vary the strength of ε_L. Two minima at the open and closed states separated by a barrier are present in the FEP of MBP (Fig. 3C) when Q_L are added with $\varepsilon_L = 2$. Thus, the ligand mediated contacts, Q_L, enable the transition to the closed conformation, which is inherently inaccessible to MBP through only the intra-protein contacts. We conclude, in agreement with experiments (Kim et al., 2013; De Boer et al., 2019), that the conformational transitions of MBP are IF-like.

Together, our results show that the conformational transitions of HisJ are CS-like while those of MBP are IF-like. We next test if structural elements within MBP, absent in HisJ (Fig. 1C and E), act to keep it in the open state.

2.4. The role of structural restraints in MBP

Several studies have demonstrated that the ligand binding affinities of MBP can be modulated by mutating the BI, a loop in the CTD which makes contacts with residues in the NTD (Fig. 1D, E, 4A), or the SH, a helix that lies behind the binding pocket making contacts with both the NTD and the CTD (Fig. 1D, E, 4A). Specifically, placing bulky residues in and near the SH (A96W and I329W) resulted in a multiple fold increase in affinity for maltose (Marvin and Hellinga, 2001b). The presence of the bulky tryptophan residues at positions A96 and I329 (Fig. 4B, cartoons below the plot) was modeled in the dSBM by increasing the distance between the Cα beads representing these residues by a factor of ~1.2, i.e., from 0.63 nm in the wild type (WT) to 0.8 nm in MBP^{WW} (also see Methods). This factor was chosen to be the average of the ratio of the sizes of the residues after and before mutation, i.e., $((r_W/r_I)+(r_W/r_A))/2$ where the subscripts denote residue identities. In this model (MBP^{WW}), a lower value of ε_L (=1.5) than WT ($\varepsilon_L = 2$) is required to induce conformational transitions. The open state minimum in the FEP (Fig. 4B) is

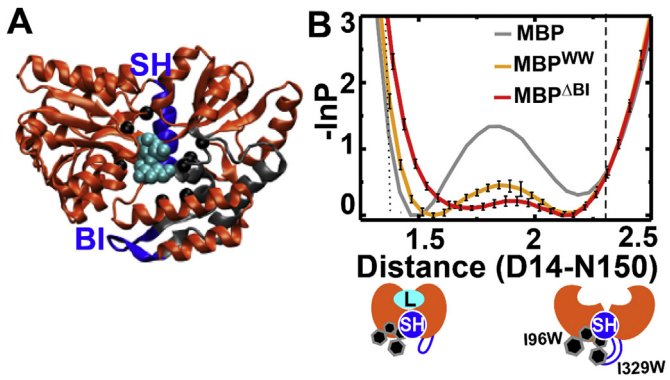

Fig. 4. Mutational manipulation of conformational transitions in MBP. (A) Ligand bound structure of MBP. Ligand is shown as cyan spheres located in the binding cleft. Although the ligand is shown here and in the cartoon in (B), it is included only implicitly into the model through the Q_L contacts. Cα atoms of residues that form the Q_L, contacts between those pairs of residues which are bridged by the ligand in the closed state, are shown as black spheres and are adjacent to the ligand. The structural restraints BI (K170-D180) and SH (K313-M330) are shown in blue. BI is flanked by protein fragments (N150–Y210) shown in grey which form several contacts with the ligand. (B) The free energy (-lnP) of MBP is plotted as a function of distance between residues D14 and N150. The vertical dashed (open state: 2.30 nm) and dotted (closed state: 1.36 nm) lines mark the distance between these residues in the respective crystal structures. The error bars shown in black represent the standard deviation of the FEP. The grey curve is reproduced from Fig. 3C and represents the FEP of the ligand induced conformational transitions of WT MBP ($\varepsilon_C = 1$, $\varepsilon_L = 2$; open state ~2.21 nm; close state ~1.50 nm). An increased distance between the Cα atoms of A96 and I329 serves as a proxy for the double mutation, A96W/I329W, in MBP^{WW}. Cartoons of the populated structures showing the position of the mutations in MBP^{WW} are shown below the basins. MBP^{WW} (orange; $\varepsilon_C = 1$, $\varepsilon_L = 1.5$; open state ~2.16 nm; close state ~1.58 nm) requires a lower strength of ligand mediated contacts to induce the conformational transition. A similar effect is seen in $MBP^{\Delta BI}$ (red; $\varepsilon_C = 1$, $\varepsilon_L = 1$; open state ~2.16 nm; close state ~1.72 nm). Both mutants also have lower barriers, i.e., the rate of conformational transitions can be modulated through mutations to residues in BI or SH.

more closed than it was in the WT because the protein has been pushed closed by increasing the distance between the SH and the NTD behind the binding pocket. Additionally, the barrier to conformational transitions is also lower. We conclude that the protein has an increased propensity to close and a lower concentration of ligand will be required to induce the conformational transition as is seen in experiment.

In a separate experiment, the effect of modulating the BI interactions was studied by deleting 4 BI residues E172, N173, K175 and Y176 (Telmer and Shilton, 2003). These modifications in combination with different mutations of the SH (M321A and Q325A) were shown to increase the ligand binding affinity by up to two orders of magnitude in MBP. To model the deletion of the BI residues, we removed eleven attractive interactions between the BI and the NTD from the open state of the WT MBP and created $MBP^{\Delta BI}$ (see Methods for details of contacts). It should be noted that, unlike in MBP^{WW}, this modification preserves the average inter-domain distance in the open state when no closed state contacts are present (Fig. S2A). However, an even lower ligand contact strength ($\varepsilon_L = 1.0$) is required to induce conformational transitions upon deletion of these contacts (Fig. 4B). BI is behind the binding pocket and its contacts with the NTD keep MBP in the open state. Some residues in the binding pocket that make up the ligand mediated contacts and promote MBP closure flank the BI (Fig. 4A). The BI and the ligand binding pocket may thus be allosterically coupled and this may be why the deletion of the BI contacts lowers the strength of ligand mediated contacts required to induce MBP to close.

In conjunction with the experimental results, the dSBM simulations indicate that BI and SH act as structural locks in the open state that resist conformational change and mutations to these regions can destabilize the open state and promote transitions to the closed state. We next examine these structural restraints in detail.

2.5. Structural modifications can modulate the mechanism of conformational transitions in HisJ and MBP

In this section, we study the effect of adding or deleting structural restraints on the ligand coupled conformational transitions of HisJ and MBP. We performed two sets of simulations: (1) A structural restraint, which mimics the SH in MBP, was added to HisJ generating $HisJ^{SH}$ and (2) BI and SH were modified to construct three dSBM variants of MBP termed $MBP^{\Delta BI}$, $MBP^{\Delta SH}$ and $MBP^{\Delta BI\Delta SH}$.

A 'spine helix'-like kink exists in HisJ but it is much shorter than the MBP SH. So, the open structure of HisJ was first modified by extending the SH by four-residues from the MBP SH. This modified structure was used to create an open state sSBM (details of all the modifications are given in Methods) to which the WT HisJ Q_C at strengths ε_C and Q_L at strengths ε_L were appended to create a new model termed $HisJ^{SH}$. While an ε_C of 1.5 is sufficient to see conformational conversion in WT, the closed state minimum is only marginally populated in $HisJ^{SH}$ even at an ε_C of 1.6 (Fig. 5A). Thus, the addition of SH does indeed stabilize the open state. Further, analogous to MBP, addition of ligand mediated contacts to $HisJ^{SH}$ (with $\varepsilon_C = 1.6$; Fig. 5A) at a strength of $\varepsilon_L = 0.5$ induced a conformational transition. However, an intermediate state, henceforth termed the semi-closed state, was also populated (Fig. S1). In order to further understand this intermediate, the inter-domain angle, i.e., the angle between the NTD and CTD (Table S2) was also used. The intermediate is characterized by an inter-domain distance of about ~1.05 nm and an inter-domain angle of 120° where the closed state angle is ~112° (~103° in the crystal structure) and the open state angle is ~135° (~135° in the crystal structure) (Fig. S1). Residues D11-A15 and S69–S72 form contacts, which are proximal to the ligand binding pocket, in the semi-closed state (Fig. S1C). Additionally, contacts made by the added SH structure remained intact in all the states (open, closed and semi-closed states). So, although an IF-like mechanism of conformational transitions is seen in $HisJ^{SH}$, this transition is not cooperative as in MBP, with a single free energy barrier between the open and the closed states. Thus, partially closed intermediates can be populated in conformational transitions if the interactions that keep the protein open are inconsistent with the interactions that the ligand makes to close it.

The structural restraints that stabilize the open state of MBP, namely BI and SH, were disengaged individually and together and three variants of MBP were generated. These modifications do not destabilize the open state and they also do not change the average inter-domain distance when no closed state contacts are present ($\varepsilon_C = 0$; Fig. S2). The conformational transitions of the first construct, $MBP^{\Delta BI}$, in the presence of ligand mediated contacts, were described in the previous section. The conformational transitions of $MBP^{\Delta BI}$ with only closed state contacts are shown in Fig. S2A. The second construct, $MBP^{\Delta SH}$, made by deleting the contacts of the SH with the NTD (see Methods for contact details), shows conformational transitions similar in nature to $MBP^{\Delta BI}$ (see Fig. S2B; no ligand mediated contacts). Here we examine the results from the third variant, $MBP^{\Delta BI\Delta SH}$, where contacts of both SH and BI were deleted. At $\varepsilon_C = 1.0$, WT MBP is in the open state, while the open-like state of $MBP^{\Delta BI\Delta SH}$ at the same ε_C has a smaller inter-domain distance and is more closed (Fig. 5B). Additionally, the $MBP^{\Delta BI\Delta SH}$ FEP nominally has two minima separated by a small barrier. The closed-like state is more open (~1.85 nm; Fig. 5B) than the closed state of the WT (~1.50 nm) with added ligand mediated contacts (Fig. 3C). When ε_C is increased further to 2.0, the $MBP^{\Delta BI\Delta SH}$ FEP shows a single minimum with a more closed state (Fig. S2C). However, ligand mediated contacts are not needed to induce the conformational transition. These results suggest that BI and SH play a key role in resisting the conformational transition and act as structural modules responsible for a IF-like mechanism in MBP. Their deletion may allow MBP to convert to a CS-like mechanism.

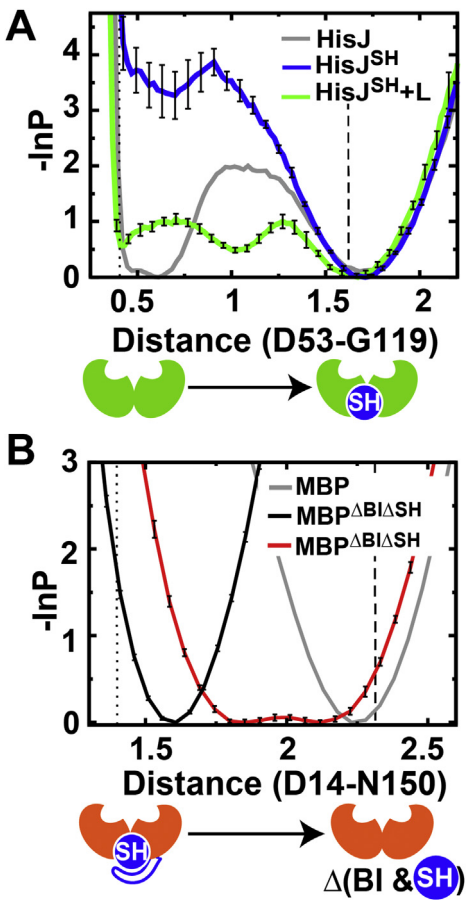

Fig. 5. Structural modifications that modulate conformational dynamics. The free energy (-lnP) is plotted as a function of distance between inter-domain residues D53 and G119 in HisJ and D14 and N150 in MBP. The vertical dashed (open state; HisJ: 1.66 nm; MBP: 2.30 nm) and dotted (closed state; HisJ: 0.39 nm; MBP: 1.36 nm) lines mark the distance between these residues in the respective crystal structures. The error bars shown in black represent the standard deviation of the FEP. Cartoons of the structural modifications made to the proteins are shown below the plots. HisJ is in green and MBP is in orange. (A) The FEP of WT HisJ ($\varepsilon_C = 1.5$; open state ~1.68 nm; closed state ~0.55 nm) is reproduced from Fig. 3A and shown in grey. Addition of SH to HisJ ($HisJ^{SH}$; blue; $\varepsilon_C = 1.6$; minimum at ~1.70 nm) restrains the conformational transition to some extent. Addition of ligand mediated contacts, Q_L, ($HisJ^{SH}$ + L; green; $\varepsilon_C = 1.6$, $\varepsilon_L = 0.5$; open state minimum at ~1.68 nm) overcomes this restraint and the conformational transition can progress to the closed state (~0.44 nm) through an intermediate (~1.05 nm) ensemble. (B) The FEP of WT MBP ($\varepsilon_C = 1.0$; only open state populated at ~2.25 nm) is reproduced from Fig. 3B and shown in grey. Deletion of BI and SH promotes the conformational transition and at the same closed state contact strength ($\varepsilon_C = 1.0$), $MBP^{\Delta BI\Delta SH}$ (red) shows a two basin FEP with an open-like state at ~2.15 nm and a closed-like basin at ~1.85 nm. $MBP^{\Delta BI\Delta SH}$ (black) further shifts to a single closed-like basin at ~1.60 nm when ε_C is increased to 2.0.

3. Discussion

3.1. dSBMs can recapitulate the mechanism of ligand coupled conformational transitions

Single SBMs, originally constructed to study protein folding, can have different levels of coarse graining. For instance, sSBMs have been constructed with all-heavy atoms (Whitford et al., 2009), 2 beads (a backbone bead and a sidechain bead) per residue (Azia and Levy, 2009; Oliveira et al., 2008; Maity and Reddy, 2018) or the Cα coarse-graining used here. Further, all contacts may be represented with the same strength and potential energy function or they may be weighted (Yadahalli and Gosavi, 2016) and may use different functional forms such as the Lennard-Jones (10–12 or 6–12) potential (Whitford et al., 2007; Cheung et al., 2005), the Coulomb interaction (Azia and Levy, 2009) or a Gaussian potential (Lammert et al., 2009). In addition to such differences, dSBMs can vary in the amount of information that they encode from the second structure: from just closed-state specific contacts (Whitford et al., 2007, 2008), similar to those calculated here, to a complete encoding of the second structure (Giri Rao et al., 2016). In fact, even for the same protein, it is important to tune the dSBM construction based on the question that needs to be answered.

Here, we set out to understand if dSBM simulations can capture the experimentally observed mechanism of conformational transitions for HisJ and MBP and in turn, if such simulations can lead to an understanding of protein structural elements that determine the mechanism. The main difference between the IF and CS mechanisms is whether the ligand binds to the open or the closed state. Thus, the effect of the ligand was specifically incorporated into the dSBM by separating closed state contacts into intra-protein closed state specific contacts, Q_C and ligand mediated contacts, Q_L (Fig. 2). The interaction strengths of these contacts were collectively scaled using a single parameter (ε_C, $\varepsilon_L \geq 1$) per contact type to effect the conformational change. However, since ε_C increased the strength of the intra-protein contacts, which are in nature similar to intra-protein open state contacts whose strength is 1, we chose ε_C to be as close to 1 as possible. With this dSBM, we observed that Q_C alone were enough to drive the conformational change in HisJ but both Q_C and Q_L were needed in MBP. Since HisJ does not require ligand mediated contacts to equilibrate between the open and closed states, its conformational transitions follow the CS mechanism. The fact that MBP undergoes conformational change only upon the inclusion of ligand mediated contacts indicates that it follows the IF mechanism. Overall, dividing contacts present only in the closed state into intra-protein contacts and ligand mediated contacts in the dSBM enabled the experimentally observed assignment of IF and CS to MBP and HisJ respectively.

3.2. Structural features that promote a specific mechanism of conformational transition

An examination of the open and closed states of HisJ and MBP provides a possible reason for the differences between their mechanisms. Both the open and the closed states of HisJ with inter-domain angles of ~135° and ~103° respectively are more closed than the open (~159°) and closed (~135°) states of MBP (Table S2). Consequently, in HisJ, the binding pocket encapsulates the ligand and in doing so forms more intra-protein contacts between the domains of the protein ($Q_C = 44$). Additionally, residues which make up Q_C line the entire binding pocket (Figs. 2 and 3A inset) making it possible for only these contacts to promote the conformational transition. In MBP, the NTD and the CTD do not come as close together in the closed state as they do in HisJ, the ligand is not completely enclosed and fewer intra-protein closed state contacts are formed ($Q_C = 16$). Further, the MBP Q_C residues are concentrated at the edges of the NTD and the CTD while the residues that make up Q_L (a proxy for the ligand) are at the center of the binding pocket (Figs. 2, 3B and 3C, insets). Hence, both the intra-protein contacts and the ligand are required to induce the conformational transition.

One possible reason for the larger inter-domain angles in MBP could be the size of the ligand. The MBP ligand, maltose, has 23 heavy (non-hydrogen) atoms as compared to the HisJ ligand, histidine, which has 11 heavy atoms. The smaller histidine may be able to access the binding pocket in not only a more compact open state but also the closed state of HisJ, leading to a CS mechanism. In contrast, MBP may need to stay open in order to avoid occluding the larger maltose and in turn, promote its binding, leading to an IF like mechanism. Additionally, the larger size of maltose may allow it to make more inter-domain contacts and enable the closure of the protein. We next examine the structural restraints that keep MBP open.

A comparison of the splay diagrams of HisJ (Fig. 1C) and MBP (Fig. 1E) shows that there are several extra structural elements, including the spine helix (SH; residues K313-M330) and the balancing interface (BI; residues K170-D180), which are present in MBP but absent in HisJ. Previous simulations and experiments have also underlined the importance of SH and BI in stabilizing the open state of MBP (Bucher et al., 2011a,b; Telmer and Shilton, 2003; Walker et al., 2010; Marvin and Hellinga, 2001; Millet et al., 2003; Mascarenhas and Kästner, 2013; Wang et al., 2012; Seo et al., 2014). The dSBM simulations (Figs. 4 and 5B) also indicate that modifying the positions or the interactions of the SH and the BI changes the nature of the conformational transition. Specifically, intact SH and BI increase the interactions between the NTD and the CTD behind the binding pocket and can potentially stabilize MBP in the open state.

3.3. Conformational transitions, free energy barriers and cooperativity

Although MBP requires ligand mediated contacts to promote conformational transitions while HisJ does not, both proteins have a free energy barrier separating the open and the closed states in models where the conformational transitions occur (Fig. 3A and C). This implies that distinct open and closed-like states are populated in both proteins, as is seen in experiment, rather than a continuum of states which progressively look more or less closed. Having distinct populated states is likely to be advantageous for both biological regulation as well as sensing where both specificity and sensitivity matter. Having a barrier implies that there is cooperative breaking and formation of multiple contacts when transitioning from one state to another. In HisJ, this cooperativity, and in turn the barrier, arises from the formation of the many Q_C contacts while destabilizing some of the open state contacts and dihedrals (Fig. 3A). In MBP, this cooperativity arises from the restraining action of the BI and SH with several of the BI and SH open state contacts being broken in the closed state. The BI (residues K170-D180), although present behind the binding site, is flanked by residues N150–Y210 in the CTD, which are part of both Q_C and Q_L and this leads to an allosteric coupling between the BI and ligand binding (Fig. 4A). Since the formation of closed and ligand mediated contacts can break the open state BI and SH contacts, the ligand binding site is optimally located to disengage the BI and SH and make the transition cooperative (Fig. 3C).

Although the HisJ and MBP mutations made here modulate the mechanism of conformational transitions (Fig. 5), they do not change the intrinsic angles of the open and closed states of the proteins. Thus, the HisJ closed state retains the numerous closed state contacts. The spine helix added to the HisJ structure can hold the protein in the open state but the SH contacts do not break during the conformational transition and a semi-closed intermediate is populated (Fig. 5A). Similarly, when the structural restraints keeping MBP open are reduced, the transition from the open to the closed state is gradual with a small free energy barrier and reduced cooperativity (Fig. 5B) because a sufficient number of closed state contacts do not exist as in HisJ. We conclude that the interactions that hold the protein in the open state have to be consistent with the closed state and ligand interactions both in position and free energies in order for there to be cooperativity and a free energy barrier in the conformational transition.

3.4. Biological implications and applications in protein design

More generally, the PBPs bind and transport their ligands to a transmembrane transporter complex on the cell membrane and can either be domains of the transporter or standalone proteins (Scheepers et al., 2016). Recent FRET experiments showed that the conformational transitions of other PBPs could also be classified as induced fit with no closed-like state being detected in the absence of the ligand (De Boer et al., 2019). A preliminary examination of these PBP structures indicates that the restraints present in these proteins are distinct from the BI and SH, with some PBPs having an extensive interface between the NTD and the CTD. dSBMs similar to the one used here should be able to identify the specific structural features as well as interactions that can modulate the mechanism of conformational transitions of these proteins.

MBP and HisJ are standalone PBPs. They bind their transporters and release ligand into the transporter channel. It is possible that the transporters make use of the PBP structural restraints, which are destabilized in the closed conformation, by binding and stabilizing them and enabling ligand release. For instance, the maltose transporter, MalF, has an unusually long P2-loop which binds MBP (Mächtel et al., 2019). The binding of this loop to the CTD of MBP could allosterically stabilize the BI and SH, lock the MBP structure back into the open state and enable ligand release. Carefully constructed dSBMs of the PBP-transporter complex should be able to identify potential regions in the complex which enable such transporter assisted ligand release.

Both mutational experiments and the simulations presented here show that mutations to the spine helix modulate the binding affinity of MBP (Figs. 4B and 5B). Further, an SH-like extension can also be used to tune the mechanism of conformational transition in HisJ (Fig. 5A). Stapled peptides, small standalone peptides in which a chemical cross-link between a pair of distal amino acids helps maintain the helical structure, have been designed to bind and inhibit target proteins which bind to helical regions (Tan et al., 2016). Our simulations indicate that stapled SH-like peptides could be designed to bind diverse PBPs on the region posterior to the binding pockets in order to modulate their ligand affinity on the fly.

4. Conclusions

We investigated the reasons behind the distinct ligand coupled conformational transition mechanisms adopted by two structurally similar proteins, HisJ and MBP. Dual structure based models (dSBMs) were built which included the open state structure and contact information from the closed state structure. Closed state specific contacts consisted of intra-protein closed state contacts and ligand mediated contacts. MD simulations of the dSBMs show that the intra-protein closed state contacts are sufficient to enable a conformational transition from the open to the closed states in HisJ indicating a conformational selection mechanism. However, ligand mediated contacts are also required to promote a transition in MBP suggesting an induced fit mechanism. Two structural elements, the spine helix (SH) and the balancing interface (BI) present on the posterior side of the ligand binding pocket increase the number of contacts between the NTD and the CTD and restrain MBP in the open state. Our simulations corroborate experiments which show that individual destabilizing mutations to the BI and SH enhance the rate of transition to the closed state. Extending this idea, we also show that eliminating the attractive interactions of the BI and SH removes the need for ligand mediated contacts and reduces the barrier to conformational transitions. Additionally, restraining HisJ in the open state by adding a SH-like structural element reduces the population of the closed state increasing the role of ligand mediated contacts in facilitating the conformational transition. Thus, short structural elements can lock a protein into the open state and impede conformational transitions. The ligand then binds the open state and provides a driving force for a transition to the closed state. The absence of structural anchors provides a protein with the hinge flexibility required to access the closed state even when ligand is not present. Thus, the preferred mechanism of conformational transitions is intrinsic to the protein structure. Overall, MD simulations of dSBMs are a computationally inexpensive method for understanding ligand binding dependent conformational transitions of proteins.

5. Methods

5.1. Dual structure-based models

We built dual structure-based models (dSBMs) to study the conformational transitions between the open and closed states of HisJ and MBP. An SBM encodes in its potential the native structure as the global

minimum (Noel and Onuchic, 2012). In a typical coarse-grained (CG) SBM each residue is treated by one CG bead located at the Cα atom. The potential energy (E) that defines the interactions between these Cα beads is given by the following expression (Lammert et al., 2009; Noel and Onuchic, 2012).

$$E = \sum_{bonds} K_r(r - r_0)^2 + \sum_{angles} K_\theta(\theta - \theta_0)^2 + \sum_{dihedrals}^{n=1,3} K_\varphi(1 - cos(n(\varphi - \varphi_0)) + \sum_{contacts} \varepsilon_1 \left(5\left(\frac{\sigma_{ij}}{r_{ij}}\right)^{12} - 6\left(\frac{\sigma_{ij}}{r_{ij}}\right)^{10}\right) + \sum_{non-contacts} \varepsilon_2 \left(\frac{\sigma}{r_{ij}}\right)^{12}$$

The first two harmonic terms are used to model bond and angular vibrations while the third term models the dihedrals in terms of a cosine function. The bond length, r_0, angle, θ_0, and dihedral, ϕ_0, are calculated from the native structure. $K_r = 100\varepsilon$, $K_\theta = 20\varepsilon$ and $K_\phi^{(1)} = 1\varepsilon$ and $K_\phi^{(3)} = 0.5\varepsilon$ are the force constants of the bond, angle and dihedral terms, respectively. These parameters ensure that the values of bonds, angles and dihedrals are maintained close to the value derived from the native structure. Here, ε is the basic energy scale and is set to 1 kJ/mol. The last two terms represent the interactions of native contacts (10–12 Lennard Jones (LJ) interaction) and non-contacts respectively. The native contacts were determined using contacts of structural units (CSU) software (Sobolev et al., 1999). σ_{ij} is the distance between residues i and j in the native state. ε_1 defines the strength of the attractive interaction for a native contact. All beads that do not form native contacts (non-contact) are defined to interact by a repulsive (excluded volume) term with $\sigma = 0.4$ nm and with $\varepsilon_2 = \varepsilon$.

In a dual SBM (dSBM), the above potential energy is extended to encode native structural data from two structures, the open and the closed states. A previous three-structure based model of MBP (Wang et al., 2012) had used backbone terms derived only from a single structure and contact information from all three structures. In order to understand if a similar model should be used here, we compared the dihedral angles between all sets of four successive Cα beads (ϕ in the equation for the potential energy, *E*) from the open and closed structures of both MBP and HisJ. In MBP, the single N-terminal residue shows a large change in dihedral angle but we disregard this change because the N-terminus is not part of a secondary structural element and is also expected to be mobile because it is the terminus. In HisJ too, a few dihedral angles present in unstructured regions such as loops and the C-terminus show large changes and can be disregarded. A few hinge dihedral angles also show a large difference between the open and the closed states in HisJ, but hinge regions are expected to be strained during the conformational transition (Whitford et al., 2007). Given the minimal change in the secondary structural content (dihedral angles) of the open and closed structures, we chose to construct a dSBM which uses backbone terms from the open structure and only includes contacts calculated from the closed structure. This is achieved by first defining the SBM of the open-state (with bond, angle, dihedral and contact terms) and then appending attractive interactions for contacts unique to the closed state to this SBM. Accordingly, we define three different sets of contacts (open state, closed state and ligand mediated) for each protein and scale their strengths of interactions, ε_O, ε_C or ε_L to achieve equal populations of both the open and the closed states. Thus, ε_1 in the equation above equals $\varepsilon_{O/C/L} \times \varepsilon$. A detailed description of the contact list calculation is given in a subsequent section. All contacts that were included in this model are listed in the SI.

5.2. Protein structures

The following crystal structures were used: HisJ: open state: PDB ID 2M8C (Chu et al., 2013); closed state: 1HSL (Yao et al., 1994) and MBP: open state: 1OMP (Sharff et al., 1992); closed state: 1ANF (Quiocho et al., 1997). MBP (1OMP) has 370 residues, however, some atoms of residue 370 were missing in the closed structure (1ANF). To keep the total number of atoms equal in both states, residue 370 was disregarded, so that both states had 369 residues. Similarly, in HisJ, out of 241 residues, three (residue 1–3) were missing in the open structure (2M8C). So, the residues were renumbered such that residue A4 was numbered A1 and therefore, both states now had 238 residues.

5.3. Contact calculation

In order to define the single SBM of the open state, its native contacts, Q_O, were calculated using the contacts of structural units (CSU) analysis (Sobolev et al., 1999) on the open structure. According to CSU, two residues i and j are in contact if the distance between them is less than the sum of their van der Waals radii and the diameter of a water molecule. The strength of the Q_O contacts, ε_O, is set to 1 and thus ε_1 for these contacts equals $\varepsilon = 1$ kJ/mol. HisJ and MBP have 655 (List S1) and 1081 (List S4) open state contacts respectively.

The recipe used to calculate the closed state (Q_C) and ligand mediated (Q_L) contacts for the two proteins closely follows that used in a dSBM of adenylate kinase (Whitford et al., 2007). In order to calculate Q_C, the closed state contacts, the ligand was removed from the PDB and CSU was used to calculate the contacts. Thus, the calculated contacts are solely intra-protein contacts. All open state contacts, i.e., those which are part of Q_O are deleted from this set. Q_C are a subset of the remaining contacts which also satisfy the following conditions (i) the contacts be inter-domain (domain boundaries are given in the SI, Table S1), i.e., they be formed between pairs of residues one each from the NTD and the CTD and (ii) their distance in the open state be at least 1.5 times their distance in the closed state. HisJ and MBP have 44 (List S2) and 16 (List S5) closed state contacts respectively. The first condition, that Q_C be inter-domain contacts, was set in order to identify a minimal set of contacts that would induce the conformational transitions. We expected that intra-domain contacts would result in localized changes but would not induce the inter-domain motion required for the conformational transition. However, a later examination found that there are no intra-domain contacts that meet the second condition (their distance in the open state be at least 1.5 times their distance in the closed state) in HisJ while only the intra-domain contacts of the floppy N-terminal residue meet the second condition in MBP. Thus, the first condition may not have been necessary for determining Q_C.

The effect of the ligand was implicitly included into the model through Q_L. First the residues in contact with the ligand were identified using the ligand protein contacts server (LPC) (Sobolev et al., 1999). All pairs of residues which met the same conditions as defined for Q_C were then identified as the ligand mediated contacts, Q_L. Thus, Q_L are inter-domain contacts whose distance in the open state is at least 1.5 times their distance in the closed state. HisJ and MBP have 15 (List S3) and 8 (List S6) ligand mediated contacts respectively. The HisJ ligand mediated contacts were not required to induce the conformational transition in the WT protein but were used in $HisJ^{SH} + L$.

The strength of the open state contacts, ε_O, is set to 1 and ε_1 in the potential energy function above equals $\varepsilon \times \varepsilon_O = 1$ kJ/mol for these contacts. The strengths of interaction of closed state and ligand mediated contacts are respectively scaled by ε_C and ε_L in order to achieve equal populations of the open and the closed states. It should be noted that the atomistic interactions underlying the coarse-grained open and closed state interactions are between similar types of atoms and should be of similar strength and nature. So, the values of ε_O, ε_C and ε_L should not be too disparate. To account for this underlying physical basis of the coarse grained interactions, we only used protein models with scaling factors greater than 2 for testing (e.g. Fig. 3B) and not as final models of the proteins (e.g. Fig. 3C). All contact lists are provided in the SI.

All open state contacts are included in Q_O and by default all contacts interact through the attractive LJ 10–12 potential given in the potential energy function. There are some open state inter-domain contacts which are also part of the closed state contact list. Such common contacts were explicitly deleted from Q_C. However, when the contact distance, σ_{ij}, of

such contacts is much shorter in the closed state than in the open state, then they could prevent the protein from closing because of the fast rising repulsive part of the LJ potential at distances less than σ_{ij}. To overcome this problem, we use a dual Gaussian (DG) potential energy function (Lammert et al., 2009) for those Q_O contacts which are also contacts in the closed state according to CSU and whose contact distance in the open state is more than 1.2 times their contact distance in the closed state. The form of this DG energy function is:

$$U_{dual-gaussian} = \varepsilon_1 \left[\left(1 + \left(\frac{\sigma_{NC}}{r_{ij}} \right)^{12} \right) \left(1 + G\left(r_{ij},\ r_1^{ij}\right)\right)\left(1 + G\left(r_{ij},\ r_2^{ij}\right)\right) - 1 \right]$$

where

$$G\left(r_{ij}, r_{n=1,2}^{ij}\right) = -exp\left[-\left(\frac{\left(r_{ij} - r_n^{ij}\right)^2}{2\sigma_n^2} \right) \right]$$

r_{ij} is the distance between the two residues i and j in contact. r^{ij}_n is the distance between the two residues in the open (n = 1) and closed (n = 2) states. σ_{NC} = 0.4 nm is the excluded volume distance and $\sigma(n = 1,2) = 0.05$ nm is the width of the Gaussian well. $\varepsilon_1 = \varepsilon_O \times \varepsilon$ is the depth of the Gaussian well and the strength of the contact. No such contacts were present in HisJ. Five such contacts, were present in MBP, listed in SI (List S4B).

5.4. Construction of mutants of HisJ and MBP

MBP^{WW} (Fig. 4B): Since each residue is represented only by its Cα atom, the mutations of A96 and I329 to the bulky W were simulated by increasing the single open state contact distance between these residues from 0.63 to 0.8 nm. The minimum of the LJ contact potential was changed by setting $\sigma_{ij} = 0.8$ nm. The interaction strength, $\varepsilon_1 = \varepsilon \times \varepsilon_O$, was not changed.

$MBP^{\Delta BI}$, $MBP^{\Delta SH}$, $MBP^{\Delta BI\Delta SH}$ (Figs. 4B and 5B, S2): All contacts between BI and the NTD were deleted to create $MBP^{\Delta BI}$ (List S7). Specific contacts between the SH and the NTD were deleted to create $MBP^{\Delta SH}$ (List S8). Both the above sets of contacts were deleted to create $MBP^{\Delta BI\Delta SH}$. Both domain definitions and the sets of deleted contacts are given in the SI. The strength of closed state contacts, ε_C, was also varied from 0 to 2.0 in steps of 0.5 in all three protein models (Fig. S2).

$HisJ^{SH}$ (Fig. 5A): The open states of HisJ (Fig. 1B) and MBP (Fig. 1D) were structurally aligned in VMD (Humphrey et al., 1996). Then 4 residues of the SH (residues M321-A324) from the aligned structure of MBP were appended as is to the pdb of HisJ and renumbered as residues M239-A242. This structure with 242 residues was relaxed with short atomistic MD simulations. This is the open state structure of $HisJ^{SH}$ and its contact map is calculated using CSU analysis (Sobolev et al., 1999) and used in simulations. Additionally, the strength ($\varepsilon^{228\text{-}238}$) of the contacts of the short helical kink (residues K228-G238; already present in WT HisJ) which precedes the added helical segment was increased to 2. The dSBM was generated by adding the WT HisJ Q_C and Q_L to this SBM. The coordinates of the Cα atoms of $HisJ^{SH}$ and its contact map are given in the SI (List S9, S10). It should be noted that the sequence of the helix extension of $HisJ^{SH}$ will likely need to be redesigned for use in experiments. Here, we do not make explicit use of the sequence, but only use the structure to understand the effect of having a spine helix on the conformational transitions of HisJ.

5.5. Conformational transition simulations of HisJ and MBP

The input (.top and.gro) files for both the open and the closed states were generated using the SMOG webserver (Noel et al., 2016) by giving contact maps and PDB files as inputs. Subsequently, the pairs and exclusion sections of the open state .top file was appropriately modified by appending either only Q_C or Q_C and Q_L contacts from the closed state .top files (Noel et al., 2010).

MD simulations were performed using a modified version of GROMACS 4.5.4, in which the Gaussian potentials were implemented (Lammert et al., 2009). The basic units of energy, temperature and distance in Gromacs are kJ/mol, K and nm, respectively. Simulations were performed in a canonical (NVT) ensemble and a stochastic dynamics integrator was used to simulate Langevin dynamics. All simulations were performed at a constant temperature of ~0.83 (in reduced units, where 1K = 0.008314 reduced units). More details on temperature estimation are available on the SMOG website (Noel et al., 2016). Each trajectory was run for 3×10^8 steps with a time step of 0.0005 ps. Simulations with conformational transitions (e.g. HisJ with Q_C or MBP with Q_C and Q_L) were performed for a sufficient number of steps such that the open and the closed states were approximately equally populated and there were at least a 100 transitions. Simulations in which only a single state was present (e.g. MBP with Q_C) were run for a similar number of steps as an equivalent simulation where conformational transitions were present.

5.6. Free energy plots (FEP) and error analysis

The distances between the Cα positions of residues D53 and G119 in HisJ (open structure: 1.66 nm, closed structure: 0.39 nm in the WT) and D14 and N150 in MBP (open structure: 2.30 nm, closed structure: 1.36 nm) were used as the reaction coordinates to monitor the conformational transitions. These specific inter-domain distances were found to best represent the transition between the open and the closed states as they demonstrate the maximum variance. Free energy profiles (FEP) were calculated by taking the negative logarithm of histogram counts of the trajectory. FEPs were then baseline shifted such that the minimum was at zero. To estimate the error in sampling, the data was divided into ~10–18 blocks such that the ratio of sample points belonging to the open and closed states was similar in each block. The standard deviation of the FEPs was calculated from these blocks.

Author contribution

Lakshmi P. Jayanthi: Software, Investigation, Writing, Funding acquisition.

Nahren Manuel Mascarenhas: Conceptualization, Methodology, Software, Investigation, Writing, Funding acquisition.

Shachi Gosavi: Conceptualization, Methodology, Writing, Supervision, Funding acquisition.

Declaration of competing interest

The authors declare that they have no known competing financial interests or personal relationships that could have appeared to influence the work reported in this paper.

Acknowledgements

This work was funded by the Tata Institute of Fundamental Research. We acknowledge support of the Department of Atomic Energy, Government of India, under project no. 12-R&D-TFR-5.04-0800 and NCBS core computational facilities, supported under 12-R&D-TFR-5.04-0900. NMM is supported by the Early Career Research Award (ECR/2016/002033) of the Science and Engineering Research Board (SERB), Govt of India and also through the DST-FIST (SR/FST/College-2017/130(c)) support to Sacred Heart College. LPJ is supported by a Women Scientist A fellowship (SR/WOS-A/CS-64/2018, 3 years, wef February 01, 2019), from the Department of Science and Technology (DST), Govt of India. SG is supported by a grant from the Government of India-SERB (EMR/2016/003885).

Appendix A. Supplementary data

Supplementary data to this article can be found online at https://doi.org/10.1016/j.crstbi.2020.08.001.

References

Aggarwal, V., Kulothungan, S.R., Balamurali, M.M., Saranya, S.R., Varadarajan, R., Ainavarapu, S.R.K., 2011. Ligand-modulated parallel mechanical unfolding pathways of maltose-binding proteins. J. Biol. Chem. 286, 28056–28065. https://doi.org/10.1074/jbc.M111.249045.

Allert, M., Rizk, S.S., Looger, L.L., Hellinga, H.W., 2004. Computational design of receptors for an organophosphate surrogate of the nerve agent soman. Proc. Natl. Acad. Sci. U.S.A. 101, 7907–7912. https://doi.org/10.1073/pnas.0401309101.

Amemiya, T., Koike, R., Kidera, A., Ota, M., 2012. PSCDB: a database for protein structural change upon ligand binding. Nucleic Acids Res. 40 https://doi.org/10.1093/nar/gkr966.

Ames, G.F.L., 1986. Bacterial periplasmic transport systems: structure, mechanism, and evolution. Annu. Rev. Biochem. 55, 397–425. https://doi.org/10.1146/annurev.bi.55.070186.002145.

Azia, A., Levy, Y., 2009. Nonnative electrostatic interactions can modulate protein folding: molecular dynamics with a grain of salt. J. Mol. Biol. 393, 527–542. https://doi.org/10.1016/j.jmb.2009.08.010.

Baxter, E.L., Jennings, P.A., Onuchic, J.N., 2012. Strand swapping regulates the iron-sulfur cluster in the diabetes drug target mitoNEET. Proc. Natl. Acad. Sci. U.S.A. 109, 1955–1960. https://doi.org/10.1073/pnas.1116369109.

Best, R.B., Chen, Y.G., Hummer, G., 2005. Slow protein conformational dynamics from multiple experimental structures: the helix/sheet transition of Arc repressor. Structure 13, 1755–1763. https://doi.org/10.1016/j.str.2005.08.009.

Bucher, D., Grant, B.J., McCammon, J.A., 2011a. Induced fit or conformational selection? the role of the semi-closed state in the maltose binding protein. Biochemistry 50, 10530–10539. https://doi.org/10.1021/bi201481a.

Bucher, D., Grant, B.J., Markwick, P.R., McCammon, J.A., 2011b. Accessing a hidden conformation of the maltose binding protein using accelerated molecular dynamics. PLoS Comput. Biol. 7 https://doi.org/10.1371/journal.pcbi.1002034.

Cai, L., Zhou, H.X., 2011. Theory and simulation on the kinetics of protein-ligand binding coupled to conformational change. J. Chem. Phys. 134 https://doi.org/10.1063/1.3561694.

Chakraborty, P., Di Cera, E., 2017. Induced fit is a special case of conformational selection. Biochemistry 56, 2853–2859. https://doi.org/10.1021/acs.biochem.7b00340.

Cheung, M.S., Klimov, D., Thirumalai, D., 2005. Molecular crowding enhances native state stability and refolding rates of globular proteins. Proc. Natl. Acad. Sci. U.S.A. 102, 4753–4758. https://doi.org/10.1073/pnas.0409630102.

Chu, B.C.H., De Wolf, T., Vogel, H.J., 2013. Role of the two structural domains from the periplasmic escherichia coli histidine-binding protein hisj. J. Biol. Chem. 288, 31409–31422. https://doi.org/10.1074/jbc.M113.490441.

Chu, B.C.H., Chan, D.I., Dewolf, T., Periole, X., Vogel, H.J., 2014. Molecular dynamics simulations reveal that apo-HisJ can sample a closed conformation. Proteins Struct. Funct. Bioinforma. 82, 386–398. https://doi.org/10.1002/prot.24396.

De Boer, M., Gouridis, G., Vietrov, R., Begg, S.L., Schuurman-Wolters, G.K., Husada, F., Eleftheriadis, N., Poolman, B., McDevitt, C.A., Cordes, T., 2019. Conformational and dynamic plasticity in substrate-binding proteins underlies selective transport in ABC importers. Elife 8. https://doi.org/10.7554/eLife.44652.

di Guana, C., Lib, P., Riggsa, P.D., Inouyeb, H., 1988. Vectors that facilitate the expression and purification of foreign peptides in Escherichia coli by fusion to maltose-binding protein. Gene 67, 21–30. https://doi.org/10.1016/0378-1119(88)90004-2.

Felder, C.B., Graul, R.C., Lee, A.Y., Merkle, H.P., Sadee, W., 1999. The venus flytrap of periplasmic binding proteins: an ancient protein module present in multiple drug receptors. AAPS PharmSci 1, 1–20. https://doi.org/10.1208/ps010202.

Ferenci, T., 1980. The recognition of maltodextrins by Escherichia coli. Eur. J. Biochem. 108, 631–636. https://doi.org/10.1111/j.1432-1033.1980.tb04758.x.

Giri Rao, V.V.H., Desikan, R., Ayappa, K.G., Gosavi, S., 2016. Capturing the membrane-triggered conformational transition of an α-helical pore-forming toxin. J. Phys. Chem. B 120, 12064–12078. https://doi.org/10.1021/acs.jpcb.6b09400.

Grant, B.J., Gorfe, A.A., McCammon, J.A., 2010. Large conformational changes in proteins: signaling and other functions. Curr. Opin. Struct. Biol. 20, 142–147. https://doi.org/10.1016/j.sbi.2009.12.004.

Greives, N., Zhou, H.X., 2014. Both protein dynamics and ligand concentration can shift the binding mechanism between conformational selection and induced fit. Proc. Natl. Acad. Sci. U.S.A. 111, 10197–10202. https://doi.org/10.1073/pnas.1407545111.

Hammes, G.G., Chang, Y.C., Oas, T.G., 2009. Conformational selection or induced fit: a flux description of reaction mechanism. Proc. Natl. Acad. Sci. U.S.A. 106, 13737–13741. https://doi.org/10.1073/pnas.0907195106.

Henzler-Wildman, K., Kern, D., 2007. Dynamic personalities of proteins. Nature 450, 964–972. https://doi.org/10.1038/nature06522.

Hu, H., Gu, Y., Xu, L., Zou, Y., Wang, A., Tao, R., Chen, X., Zhao, Y., Yang, Y., 2017. A genetically encoded toolkit for tracking live-cell histidine dynamics in space and time. Sci. Rep. 7 https://doi.org/10.1038/srep43479.

Huang, W., Blinov, N., Wishart, D.S., Kovalenko, A., 2015. Role of water in ligand binding to maltose-binding protein: insight from a new docking protocol based on the 3D-RISM-KH molecular theory of solvation. J. Chem. Inf. Model. 55, 317–328. https://doi.org/10.1021/ci500520q.

Humphrey, W., Dalke, A., Schulten, K., 1996. VMD: visual molecular dynamics. J. Mol. Graph. 14, 33–38. https://doi.org/10.1016/0263-7855(96)00018-5.

Kapust, R.B., Waugh, D.S., 1999. Escherichia coli maltose-binding protein is uncommonly effective at promoting the solubility of polypeptides to which it is fused. Protein Sci. 8, 1668–1674. https://doi.org/10.1110/ps.8.8.1668.

Kim, E., Lee, S., Jeon, A., Choi, J.M., Lee, H.S., Hohng, S., Kim, H.S., 2013. A single-molecule dissection of ligand binding to a protein with intrinsic dynamics. Nat. Chem. Biol. 9, 313–318. https://doi.org/10.1038/nchembio.1213.

Kondo, H.X., Okimoto, N., Morimoto, G., Taiji, M., 2011. Free-energy landscapes of protein domain movements upon ligand binding. J. Phys. Chem. B 115, 7629–7636. https://doi.org/10.1021/jp111902t.

Koshland, D.E., Nemethy, J.G., Filmer, D., 1966. Comparison of experimental binding data and theoretical models in proteins containing subunits. Biochemistry 5, 365–385. https://doi.org/10.1021/bi00865a047.

Kotamarthi, H.C., Narayan, S., Ainavarapu, S.R.K., 2014. Mechanical unfolding of ribose binding protein and its comparison with other periplasmic binding proteins. J. Phys. Chem. B 118, 11449–11454. https://doi.org/10.1021/jp507463q.

Lammert, H., Schug, A., Onuchic, J.N., 2009. Robustness and generalization of structure-based models for protein folding and function. Proteins Struct. Funct. Bioinforma. 77, 881–891. https://doi.org/10.1002/prot.22511.

Lukman, S., Verma, C.S., Fuentes, G., 2009. Exploiting protein intrinsic flexibility in drug design. In: Han, K., Zhang, X., Yang, M. (Eds.), Protein Conformational Dynamics. Advances in Experimental Medicine and Biology, vol. 805. Springer, Cham, pp. 245–269. https://doi.org/10.1007/978-3-319-02970-2_11.

Mächtel, R., Narducci, A., Griffith, D.A., Cordes, T., Orelle, C., 2019. An integrated transport mechanism of the maltose ABC importer. Res. Microbiol. 170, 321–337. https://doi.org/10.1016/j.resmic.2019.09.004.

Maity, H., Reddy, G., 2018. Thermodynamics and kinetics of single-chain monellin folding with structural insights into specific collapse in the denatured state ensemble. J. Mol. Biol. 430, 465–478. https://doi.org/10.1016/j.jmb.2017.09.009.

Marvin, J.S., Hellinga, H.W., 2001a. Conversion of a maltose receptor into a zinc biosensor by computational design. Proc. Natl. Acad. Sci. U.S.A. 98, 4955–4960. https://doi.org/10.1073/pnas.091083898.

Marvin, J.S., Hellinga, H.W., 2001b. Manipulation of ligand binding affinity by exploitation of conformational coupling. Nat. Struct. Biol. 8, 795–798. https://doi.org/10.1038/nsb0901-795.

Mascarenhas, N.M., Kästner, J., 2013. How maltose influences structural changes to bind to maltose-binding protein: results from umbrella sampling simulation. Proteins Struct. Funct. Bioinforma. 81, 185–198. https://doi.org/10.1002/prot.24174.

Medintz, I.L., Deschamps, J.R., 2006. Maltose-binding protein: a versatile platform for prototyping biosensing. Curr. Opin. Biotechnol. 17, 17–27. https://doi.org/10.1016/j.copbio.2006.01.002.

Miller, D.M., Olson, J.S., Pflugrath, J.W., Quiocho, F.A., 1983. Rates of ligand binding to periplasmic proteins involved in bacterial transport and chemotaxis. J. Biol. Chem. 258, 13665–13672.

Millet, O., Hudson, R.P., Kay, L.E., 2003. The energetic cost of domain reorientation in maltose-binding protein as studied by NMR and fluorescence spectroscopy. Proc. Natl. Acad. Sci. U.S.A. 100, 12700–12705. https://doi.org/10.1073/pnas.2134311100.

Monod, J., Wyman, J., Changeux, J.P., 1965. On the nature of allosteric transitions: a plausible model. J. Mol. Biol. 12, 88–118. https://doi.org/10.1016/S0022-2836(65)80285-6.

Muñoz, V., 2007. Conformational dynamics and ensembles in protein folding. Annu. Rev. Biophys. Biomol. Struct. 36, 395–412. https://doi.org/10.1146/annurev.biophys.36.040306.132608.

Nadler, D.C., Morgan, S.A., Flamholz, A., Kortright, K.E., Savage, D.F., 2016. Rapid construction of metabolite biosensors using domain-insertion profiling. Nat. Commun. 7 https://doi.org/10.1038/ncomms12266.

Noel, J.K., Onuchic, J.N., 2012. The many faces of structure-based potentials: from protein folding landscapes to structural characterization of complex biomolecules. In: Dokholyan, N. (Ed.), Computational Modeling of Biological Systems. Biological and Medical Physics, Biomedical Engineering. Springer, Boston, MA, pp. 31–54. https://doi.org/10.1007/978-1-4614-2146-7_2.

Noel, J.K., Whitford, P.C., Sanbonmatsu, K.Y., Onuchic, J.N., 2010. SMOG@ctbp: simplified deployment of structure-based models in GROMACS. Nucleic Acids Res. 38 https://doi.org/10.1093/nar/gkq498.

Noel, J.K., Levi, M., Raghunathan, M., Lammert, H., Hayes, R.L., Onuchic, J.N., Whitford, P.C., 2016. Smog 2: a versatile software package for generating structure-based models. PLoS Comput. Biol. 12 https://doi.org/10.1371/journal.pcbi.1004794.

Okazaki, K.I., Takada, S., 2008. Dynamic energy landscape view of coupled binding and protein conformational change: induced-fit versus population-shift mechanisms. Proc. Natl. Acad. Sci. U.S.A. 105, 11182–11187. https://doi.org/10.1073/pnas.0802524105.

Okazaki, K.I., Koga, N., Takada, S., Onuchic, J.N., Wolynes, P.G., 2006. Multiple-basin energy landscapes for large-amplitude conformational motions of proteins: structure-based molecular dynamics simulations. Proc. Natl. Acad. Sci. U.S.A. 103, 11844–11849. https://doi.org/10.1073/pnas.0604375103.

Oliveira, L.C., Schug, A., Onuchic, J.N., 2008. Geometrical features of the protein folding mechanism are a robust property of the energy landscape: a detailed investigation of several reduced models. J. Phys. Chem. B 112, 6131–6136. https://doi.org/10.1021/jp0769835.

Paul, F., Weikl, T.R., 2016. How to distinguish conformational selection and induced fit based on chemical relaxation rates. PLoS Comput. Biol. 12 https://doi.org/10.1371/journal.pcbi.1005067.

Paul, S., Banerjee, S., Vogel, H.J., 2017. Ligand binding specificity of the Escherichia coli periplasmic histidine binding protein. HisJ, Protein Sci. 26, 268–279. https://doi.org/10.1002/pro.3079.

Quiocho, F.A., Ledvina, P.S., 1996. Atomic structure and specificity of bacterial periplasmic receptors for active transport and chemotaxis: variation of common themes. Mol. Microbiol. 20, 17–25. https://doi.org/10.1111/j.1365-2958.1996.tb02484.x.

Quiocho, F.A., Spurlino, J.C., Rodseth, L.E., 1997. Extensive features of tight oligosaccharide binding revealed in high-resolution structures of the maltodextrin

transport/chemosensory receptor. Structure 5, 997–1015. https://doi.org/10.1016/S0969-2126(97)00253-0.
Ramírez-Sarmiento, C.A., Noel, J.K., Valenzuela, S.L., Artsimovitch, I., 2015. Interdomain contacts control native state switching of RfaH on a dual-funneled landscape. PLoS Comput. Biol. 11 https://doi.org/10.1371/journal.pcbi.1004379.
Ribeiro, L.F., Amarelle, V., Ribeiro, L.F.C., Guazzaroni, M.E., 2019. Converting a periplasmic binding protein into a synthetic biosensing switch through domain insertion. BioMed Res. Int. 2019 https://doi.org/10.1155/2019/4798793.
Scheepers, G.H., Lycklama a Nijeholt, J.A., Poolman, B., 2016. An updated structural classification of substrate-binding proteins. FEBS Lett. 590, 4393–4401. https://doi.org/10.1002/1873-3468.12445.
Seo, M.H., Park, J., Kim, E., Hohng, S., Kim, H.S., 2014. Protein conformational dynamics dictate the binding affinity for a ligand. Nat. Commun. 5 https://doi.org/10.1038/ncomms4724.
Sharff, A.J., Rodseth, L.E., Spurlino, J.C., Quiocho, F.A., 1992. Crystallographic evidence of a large ligand-induced hinge-twist motion between the two domains of the maltodextrin binding protein involved in active transport and chemotaxis. Biochemistry 31, 10657–10663. https://doi.org/10.1021/bi00159a003.
Sharff, A.J., Quiocho, F.A., Rodseth, L.E., Quiocho, F.A., 1993. Refined 1.8-å structure reveals the mode of binding of β-cyclodextrin to the maltodextrin binding protein. Biochemistry 32, 10553–10559. https://doi.org/10.1021/bi00091a004.
Silva, D.A., Bowman, G.R., Sosa-Peinado, A., Huang, X., 2011. A role for both conformational selection and induced fit in ligand binding by the Lao protein. PLoS Comput. Biol. 7 https://doi.org/10.1371/journal.pcbi.1002054.
Sobolev, V., Sorokine, A., Prilusky, J., Abola, E.E., Edelman, M., 1999. Automated analysis of interatomic contacts in proteins. Bioinformatics 15, 327–332. https://doi.org/10.1093/bioinformatics/15.4.327.
Stockner, T., Vogel, H.J., Tieleman, D.P., 2005. A salt-bridge motif involved in ligand binding and large-scale domain motions of the maltose-binding protein. Biophys. J. 89, 3362–3371. https://doi.org/10.1529/biophysj.105.069443.
Tan, Y.S., Lane, D.P., Verma, C.S., 2016. Stapled peptide design: principles and roles of computation. Drug Discov. Today 21, 1642–1653. https://doi.org/10.1016/j.drudis.2016.06.012.
Tang, C., Schwieters, C.D., Clore, G.M., 2007. Open-to-closed transition in apo maltose-binding protein observed by paramagnetic NMR. Nature 449, 1078–1082. https://doi.org/10.1038/nature06232.
Telmer, P.G., Shilton, B.H., 2003. Insights into the conformational equilibria of maltose-binding protein by analysis of high affinity mutants. J. Biol. Chem. 278, 34555–34567. https://doi.org/10.1074/jbc.M301004200.
Walker, I.H., Hsieh, P.C., Riggs, P.D., 2010. Mutations in maltose-binding protein that alter affinity and solubility properties. Appl. Microbiol. Biotechnol. 88, 187–197. https://doi.org/10.1007/s00253-010-2696-y.
Wang, Y., Tang, C., Wang, E., Wang, J., 2012. Exploration of multi-state conformational dynamics and underlying global functional landscape of maltose binding protein. PLoS Comput. Biol. 8 https://doi.org/10.1371/journal.pcbi.1002471.
Weikl, T.R., Von Deuster, C., 2009. Selected-fit versus induced-fit protein binding: kinetic differences and mutational analysis. Proteins Struct. Funct. Bioinforma. 75, 104–110. https://doi.org/10.1002/prot.22223.
Whitford, P.C., Miyashita, O., Levy, Y., Onuchic, J.N., 2007. Conformational transitions of adenylate kinase: switching by cracking. J. Mol. Biol. 366, 1661–1671. https://doi.org/10.1016/j.jmb.2006.11.085.
Whitford, P.C., Gosavi, S., Onuchic, J.N., 2008. Conformational transitions in adenylate kinase: allosteric communication reduces misligation. J. Biol. Chem. 283, 2042–2048. https://doi.org/10.1074/jbc.M707632200.
Whitford, P.C., Noel, J.K., Gosavi, S., Schug, A., Sanbonmatsu, K.Y., Onuchic, J.N., 2009. An all-atom structure-based potential for proteins: bridging minimal models with all-atom empirical forcefields. Proteins Struct. Funct. Bioinforma. 75, 430–441. https://doi.org/10.1002/prot.22253.
Wolf, A., Shaw, E.W., Nikaido, K., Ames, G.F.L., 1994. The histidine-binding protein undergoes conformational changes in the absence of ligand as analyzed with conformation-specific monoclonal antibodies. J. Biol. Chem. 269, 23051–23058.
Yadahalli, S., Gosavi, S., 2016. Functionally relevant specific packing can determine protein folding routes. J. Mol. Biol. 428, 509–521. https://doi.org/10.1016/j.jmb.2015.12.014.
Yao, N., Trakhanov, S., Quiocho, F.A., 1994. Refined 1.89-å structure of the histidine-binding protein complexed with histidine and its relationship with many other active transport/chemosensory proteins. Biochemistry 33, 4769–4779. https://doi.org/10.1021/bi00182a004.
Zhou, H.X., 2010. From induced fit to conformational selection: a continuum of binding mechanism controlled by the timescale of conformational transitions. Biophys. J. 98 https://doi.org/10.1016/j.bpj.2009.11.029.